Gain-Scheduled Control of Modular Battery for Thermal and SOC Balancing ⋆

Faisal Altaf * **Bo Egardt** *

* *Department of Signals and Systems, Chalmers University of Technology, Gothenburg, Sweden (e-mail: faisal.altaf@chalmers.se).*

Abstract: This paper proposes a simple constrained proportional controller with gain scheduling for simultaneous thermal and SOC balancing of a multilevel converter based modular battery. The proposed balancing controller is devised by investigating structural properties of constrained linear quadratic (LQ) model predictive controller (MPC) introduced in our earlier study. This investigation reveals a particular factorization of time-varying control gain matrices, which leads to approximation of matrix gains as scalar gains under the assumption of small parametric variations among battery cells. The gains are scheduled in load current. This special structure enables the identification of two dominant operational modes of the balancing controller: SOC balancing mode in low to medium load current range and thermal balancing mode in high current range. This study also proposes a simple algorithm for control projection on constraint polytope. The proposed balancing controller is tested in simulations for a modular battery with four significantly mismatched cells. The performance is comparable to MPC, which uses true battery parameters. The performance and the simplicity of the controller make it attractive for real-time implementation in large battery packs.

Keywords: Batteries, cell balancing, SOC balancing, thermal balancing, modular battery, multilevel converters, gain scheduling, LQ Control, model predictive control.

1. INTRODUCTION

The transportation is going through a critical transition phase to improve energy efficiency and reduce CO_2 emissions. The battery-powered electrified vehicles (xEVs) are one of the competitive solutions. The main drawback of xEVs is the high initial cost and relatively short lifetime of battery pack. The lithium-ion battery system is currently emerging as dominant technology for future xEVs. However, like all other battery types, the ageing rate of each Li-ion cell is greatly affected by various factors like state-of-charge (SOC) level, depth-of-discharge (DOD), temperature, and c-rate etc as shown by Vetter et al. (2005); Wang et al. (2011); Bandhauer et al. (2011), and Groot (2014). In short, the cells in the string being stored or cycled at higher SOC-level, DOD and temperature may age faster than those at lower SOC, DOD, and temperature, resulting in nonuniform ageing of cells. The cell imbalance and nonuniform ageing are also tightly coupled, which may lead to a vicious cycle resulting in the premature end of battery life. In addition to nonuniform ageing, the SOC imbalance also has a detrimental impact on the total usable capacity of the battery, see review papers by Lu et al. (2013) and Altaf et al. (2014) for details. Thermal, SOC, and DOD imbalance is inevitable in battery packs of xEVs due to variations in cell parameters and operating conditions, see Dubarry et al. (2010); Mahamud and Park (2011). Thus, thermal and SOC balancer is very critical for optimal performance of automotive batteries. The SOC balancing can be achieved using various types of passive or active SOC balancers, see Gallardo-Lozano et al. (2014); Cao et al. (2008), whereas thermal balancing can potentially be achieved using reciprocating air-flow as proposed by Mahamud and Park (2011).

The notion of *simultaneous thermal and SOC balancing* using a single active balancing device was introduced in our previous work, see Altaf et al. (2012, 2013); Altaf (2014). A similar kind of conceptual study has also been carried out by Barreras et al. (2014). Thermal and SOC balancing are two tightly coupled and somewhat conflicting objectives, but it is possible to achieve both simultaneously in average sense subject to load variations and *surplus battery voltage* (Altaf et al. (2014)). In addition, it requires a special balancing device, like multilevel converter (MLC) (Malinowski et al. (2010)), which enables *bidirectional power flow* from each battery module to achieve non-uniform load scheduling. The MLC-based *modular battery* consists of n cascaded power units (PUs), each containing a smaller battery unit and a full-bridge dc-dc converter. The modular battery is reconfigurable and provides a large redundancy in the voltage synthesis, which gives extra degree-of-freedom in control.

The modular battery has multiple electro-thermal control objectives including thermal balancing, SOC balancing, and terminal voltage control. In Altaf et al. (2015b,a), a linear quadratic model predictive control (LQ MPC) scheme is proposed, which achieves the balancing objectives by using only one-step prediction. The control scheme is based on the decomposition of controller into

⋆ The work was supported by the Chalmers Energy Initiative.

two orthogonal components, one for voltage control and the other for balancing control. The *voltage control problem* is a simple minimum norm problem, whereas the *balancing problem* is formulated as a *control-constrained LQ MPC* problem, which is solved in two stages. The *first stage* issues an optimal balancing control policy (control gains) by solving a standard time-varying unconstrained LQ problem. The *second stage* generates feasible control actions by doing Euclidean projection of unconstrained LQ controls on a time-varying control constraint polytope.

This paper is an extension of Altaf et al. (2015a). The main purpose is to further simplify the balancing controller. The idea is to approximate the LQ control gains by studying their structural properties and solve control projection problem by a simple algorithm. This leads to a simple proportional controller with load current dependent scalar gains. The controller can be easily implemented online as it is based on evaluating simple gain polynomials and doing straightforward iterations for Euclidean projection instead of strictly solving an optimization problem. In addition, this study completely unfolds the internal working and reveals two dominant operational modes of the balancing controller, which leads to very simple balancing rules based on load current magnitude.

Two proposed controllers (one based on the gain polynomials and other based on the balancing rules) are evaluated and compared to MPC through simulations. We assume Toyota Prius PHEV, running in EV mode for *US06* drive cycle, as load for an air-cooled modular battery consisting of four cells. To analyze the effectiveness of the controllers, we assume significant variations among resistances, capacities, and initial SOCs of cells.

The paper is organized as follows. The modeling of MLC-based modular battery and the previous LQ MPC scheme are briefly summarized in sections 2 and 3 respectively. The proposed proportional controller is presented in section 4. The simulation results are discussed in section 5 and conclusions are drawn in section 6.

2. MODULAR BATTERY: MODELING

The electro-thermal model of an air-cooled modular battery is presented in this section, see Altaf et al. (2012, 2013, 2015a) and Altaf (2014) for modeling details.

2.1 MLC-based Modular Battery: Overview

The (cascaded h-bridge) MLC-based modular battery, supplying voltage $v_L(t) \in [0, v_{L,\max}] \subseteq \mathbb{R}_+$ to a variable load with current demand $i_L(t) \in [i_{L,\min}, i_{L,\max}] \subseteq \mathbb{R}$, is shown in Figure 1. The MLC consists of n series-connected PUs, each containing an ideal full-bridge (FB) and an isolated Cell$_i$. This modular structure allows four quadrant operation in i_L–v_{Li} plane, which enables control of bidirectional power flow from each Cell$_i$ using control variables u_i (duty cycle). In this study, we assume positively constrained control i.e. $u_(t) \in [0,1]$ (so-called *unipolar control scheme*). This scheme does not allow polarity inversion of any cell in the string, which simply implies that at any time instant, either all cells are charging (for $i_L(t) < 0$) or all are discharging (for $i_L(t) > 0$).

The *averaged signals* on two ports of ideal FB$_i$ (see Fig. 1) are linearly related through duty cycle $u_i(t)$ as follows

$$i_{Bi}(t) = i_L(t)u_i(t), \quad v_{Li}(t) = d_{vi}(t)u_i(t), \tag{1}$$

where i_L and v_{Li} are the terminal current and voltage of PU$_i$ respectively, i_{Bi} is the current through Cell$_i$, and

$$d_{vi}(t) = v_{oci} - i_L(t)R_{ei} \tag{2}$$

is the ON-time terminal voltage of Cell$_i$, where v_{oci} is OCV and R_{ei} is internal resistance. The terminal voltage and power of the modular battery are given by $v_L(t) = \sum_{i=1}^{n} v_{Li}(t)$ and $P_L(t) = \sum_{i=1}^{n} P_{Li}(t)$ respectively, where $P_{Li}(t) = v_{Li}(t)i_L(t)$ is the power output from each PU$_i$.

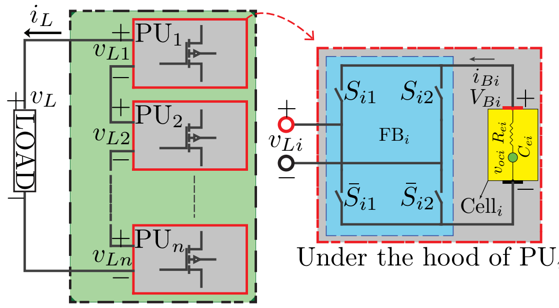

Fig. 1. MLC-based n-cell modular battery in green box.

2.2 Electro-thermal Model of Modular Battery

The electrical dynamics of cells is studied using the *simple cell model* (OCV-R), see Hu et al. (2012). The thermal dynamics of air-cooled battery is modeled using lumped capacitance and flow network modeling approach, see Mahamud and Park (2011); Lin et al. (2013a,b). The model considers only cell surface temperature with constant coolant temperature and speed at inlet. All internal parameters of cells are assumed constant. Under these assumptions, the electro-thermal model of any Cell$_i$ of the modular battery for a given load current $i_L(t)$ is given by

$$\dot{\xi}_i(t) = -\frac{1}{3600C_{ei}} i_L(t)u_i(t), \tag{3a}$$

$$\dot{T}_{si}(t) = \sum_{j=1}^{i} a_{tij}T_{sj}(t) + \frac{R_{ei}}{C_{si}} i_L^2(t)u_i(t) + w_{ti}T_{f0}, \tag{3b}$$

$$v_{Li}(t) = d_{vi}(t)u_i(t), \tag{3c}$$

where temperature, $T_{si}(t)$, and SOC, $\xi_i(t)$, are states, T_{f0} is the constant inlet fluid temperature (measured disturbance), $v_{Li}(t)$ is the terminal voltage of PU$_i$, and $d_{vi}(t)$, given by (2), is considered as a time-varying feedthrough gain. The parameter C_{ei} is the charge capacity, R_{ei} is the resistance, and C_{si} is the heat capacity of Cell$_i$. The coefficients $a_{tij} = f(\alpha,\beta)a_{si}$ and $w_{t=} - \sum_{j=1}^{i} a_{tij}$ are thermal circuit parameters for unidirectional coolant flow, where $f(\alpha,\beta)$ is a rational function of α_i:s and β_i:s and w_{ti} describes influence of T_{f0} on Cell$_i$, see Altaf et al. (2015a) for definition. All other parameters are defined in Table 1.

Using (3a)–(3c) as basic building block and treating T_{f0} as a dummy state, the continuous-time (CT) electro-thermal model of a n-cell modular battery is given by the following standard linear time-varying (LTV) state-space system

$$\dot{x}(t) = Ax(t) + B(i_L(t))u(t), \tag{4a}$$

$$y(t) = Cx(t) + D(i_L(t))u(t). \tag{4b}$$

Here $x(t) = \left[\xi^{\mathrm{T}}(t)\ \vartheta^{\mathrm{T}}(t)\right]^{\mathrm{T}} \in \mathbb{R}^{2n+1}$ is the state vector, $\xi(t) = [\xi_1 \cdots \xi_n]^{\mathrm{T}} \in \mathbb{R}^n$, $\vartheta(t) = \left[T_s^{\mathrm{T}}\ T_{f0}\right]^{\mathrm{T}} \in \mathbb{R}^{n+1}$ is an augmented thermal state with $T_s(t) = [T_{s1} \cdots T_{sn}]^{\mathrm{T}} \in \mathbb{R}^n$, $u(t) = [u_1 \cdots u_n]^{\mathrm{T}} \in \mathbb{R}^n$ is the control input, $y(t) = \left[\vartheta^{\mathrm{T}}(t)\ v_L(t)\right]^{\mathrm{T}} \in \mathbb{R}^{n+2}$ is the output, and

$$v_L(t) = \sum_{i=1}^{n} v_{Li} = \sum_{i=1}^{n} d_{vi}(t)u_i = D_v(t)u(t). \tag{5}$$

All the state-space matrices are defined in Appendix A. The discrete-time (DT) state-space model is given by

$$x(k+1) = A_d x(k) + B_d(i_L(k))u(k), \tag{6a}$$
$$y(k) = Cx(k) + D(i_L(k))u(k), \tag{6b}$$

where A_d and $B_d(k)$ are obtained using Euler approximation assuming $i_L(k)$ to be constant during each sampling interval $[kh, (k+1)h]$ where h is a sampling step size.

Table 1. Definition of Cell/Coolant Parameters

Parameters	Expression	Units
OCV of Cell$_i$	v_{oci}	V
Electrical Resistance	R_{ei}	Ω
Charge Capacity	C_{ei}	Ah
Thermal Resistance	R_{ui}	KW^{-1}
Air Density	ρ_f	$kg\,m^{-3}$
Air Specific Heat Capacity	c_{pf}	$JK^{-1}kg^{-1}$
Air Volumetric Flow Rate	$\dot{V}_f$	m^3s^{-1}
Air Thermal Conductance	$c_f = \rho_f c_{pf} \dot{V}_f$	WK^{-1}
Temperature Coeff.	$a_{si} = (C_{si}R_{ui})^{-1}$	s^{-1}
Thermal Coupling Coeff.	$\alpha_i = R_{ui}c_f$	Unitless
Thermal Coupling Coeff.	$\beta_i = -1 + \alpha_i$	Unitless

2.3 Control Constraint Set

The unipolar control scheme imposes control constraint $u_i(k) \in [0, 1]$ for each Cell$_i$. Therefore, the control constraint set of n-cell modular battery is given by

$$\mathcal{U} = \{u(k) | H_u u \le h_u,\ \forall k\}, \tag{7}$$

for suitably defined H_u and h_u.

3. LQ MPC CONTROL SCHEME: OVERVIEW

In this section, we give an overview of 1-step LQ MPC scheme proposed by Altaf et al. (2015b,a). The electro-thermal control objectives include simultaneous thermal and SOC balancing (balancing problem) as well as terminal voltage control (voltage regulation problem) of modular battery. The proposed scheme prioritizes the load voltage regulation (supply = demand). The balancing is treated as secondary objective, which is achieved by optimally using any redundancy available in the modular battery after meeting power demand. The control strategy is mainly developed based on the decomposition of controller into two *orthogonal components* as follows

$$u(k) = u_v(k) + u_b(k) \in \mathcal{U}, \tag{8}$$

where control $u_v(k) \in \left(\mathcal{U} \cap \mathcal{N}(D_v(k))^{\perp}\right)$ is for voltage control and $u_b(k) \in \mathcal{U}_b(k) \subseteq \mathcal{N}(D_v(k))$ is for balancing control where $\mathcal{U}_b(k)$ (so-called truncated null-space) is a balancing control constraint polytope (defined in (B.3)), $\mathcal{N}(D_v(k))$ is the nullspace of $D_v(k)$ and $\mathcal{N}(D_v(k))^{\perp}$ is the orthogonal complement of $\mathcal{N}(D_v(k))$, see Appendix B for definitions. The proposed orthogonal decomposition guarantees the voltage constraint while giving the possibility of simultaneous thermal and SOC balancing. The block diagram of control scheme is shown in Figure 2(a). The voltage and balancing controllers are summarized below, see Altaf et al. (2015a) for details.

3.1 Voltage Controller: Minimum Norm Problem

The feedforward voltage control $u_v(k)$, for a known load demand $(i_L(k), v_{Ld}(k))$, is given by (Altaf et al. (2015a,b))

$$u_v(k) = (D_v(k))^{\dagger}\, v_{Ld}(k), \tag{9}$$

where $(D_v)^{\dagger} = D_v^{\mathrm{T}}\left(D_v D_v^{\mathrm{T}}\right)^{-1}$ is a right pseudo-inverse of D_v. The solution $u_v(k) \in \mathcal{R}(D_v(k)^{\mathrm{T}})$ is guaranteed to be inside $\mathcal{U}$ for load demands $i_L(k) \in [i_{L\min}, i_{L\max}]$ and $v_{Ld}(k) \in [0, v_{Ld\max}]$ with appropriately defined limits $i_{L\min}, i_{L\max}$, and $v_{Ld\max} < v_{L\max}(k)$.

3.2 Balancing Controller: LQ MPC Scheme

The main objective is to design $u_b(k) \in \mathcal{U}_b(k) \subseteq \mathcal{N}(D_v)$ such that *SOC and temperature errors* for each Cell$_i$

$$e_{\xi_i}(k) = \xi_i(k) - \bar{\xi}(k), \tag{10}$$
$$e_{T_{si}}(k) = T_{si}(k) - \bar{T}_s(k), \tag{11}$$

are minimized without increasing average battery temperature, $\sum_{k=1}^{N_d} \bar{T}_s(k)/N_d$, over driving horizon N_d relative to that of unbalanced battery. Here $\bar{\xi}(k) = \frac{1}{n}1_n^{\mathrm{T}}\xi(k)$ and $\bar{T}_s(k) = \frac{1}{n}1_n^{\mathrm{T}}T_s(k)$ are instantaneous *mean SOC* and *mean temperature* of the modular battery and considered as reference signals here. The objective is achieved by solving, in the MPC framework, the following 1-step *control-constrained LQ* problem at each time step.

$$\begin{aligned} \text{minimize}\quad & \left[\|x(k+1)\|^2_{\bar{P}_x} + \|\rho_b(k)\|^2_{R_{\rho_b}}\right] \\ \text{subject to}\quad & x(k+1) = A_d x(k) + \bar{B}_d(k)\rho_b(k), \\ & u_b(k) = V_{\mathrm{n}}(i_L(k))\rho_b(k) \in \mathcal{U}_b(k), \end{aligned} \tag{P-I}$$

for given $x(k)$, $i_L(k)$, and $u_v(k)$, with optimization variables $x(k+1)$ and $\rho_b(k) \in \mathbb{R}^{n-1}$ (null-space coefficient vector that is equal to last $n-1$ elements of $u_b(k)$) where $V_{\mathrm{n}}(i_L(k))$, defined in (B.2), is a null-space basis matrix and $\bar{B}_d(k) = B_d(i_L(k)) \cdot V_{\mathrm{n}}(i_L(k))$. Note that $\bar{P}_x$ is a block-diagonal matrix that maps battery's state $x(k+1)$ to quadratic costs $q_E e^2_{\xi_i}(k+1)$ (SOC deviation penalty) + $q_T e^2_{T_{si}}(k+1)$ (temperature deviation penalty) + $q_{\bar{T}}\bar{T}_s^2(k+1)$ (temperature rise penalty) for all cells. The matrix $R_{\rho_b}(k) = \gamma_4 V_n^{\mathrm{T}}(i_L(k))R_{u_b}V_{\mathrm{n}}(i_L(k))$, with R_{u_b} as a penalty on u_b, is a penalty weight for $\rho_b(k)$.

The problem (P-I) is solved in *two stages*:

(1) *Unconstrained LQ Problem:* Firstly, we solve unconstrained LQ problem to find unconstrained control

$$\rho_b^u(k) = K_{\rho_b}(k)x(k), \tag{12}$$

where superscript 'u' stands for 'unconstrained' and the gain $K_{\rho_b}(k)$ is given by single Riccati recursion

$$K_{\rho_b}(k) = -[R_{\rho_b}(k) + \bar{B}_d^{\mathrm{T}}(k)\bar{P}_x\bar{B}_d(k)]^{-1}\bar{B}_d^{\mathrm{T}}(k)\bar{P}_x A_d, \tag{13}$$

Then, using (12), we recover full balancing control

$$u_b^u(k) = K_{u_b}(k)x(k), \tag{14}$$

where $K_{u_b}(k) = V_n(k)K_{\rho_b}(k)$. The total unconstrained control is given by

$$u^u(k) = u_v(k) + u_b^u(k). \tag{15}$$

Note that the balancing control policy u_b^u uses battery state as feedback and battery load (i_L and u_v) as feedforward to achieve balancing objectives.

(2) *Constrained Control via Projection:* Secondly, we compute constrained control action by projecting $u_b^u(k)$ on the constraint set $\mathcal{U}_b(k)$.

$$\begin{aligned} \text{minimize} \quad & \|u_b(k) - u_b^u(k)\|^2 \\ \text{subject to} \quad & u_b(k) \in \mathcal{U}_b(k) \end{aligned} \tag{P-II}$$

where the time-varying set $\mathcal{U}_b(k)$ is defined in (B.3).

4. RULE-BASED PROPORTIONAL BALANCING CONTROLLER WITH GAIN-SCHEDULING

From (12), it is straightforward to verify that the complete balancing control structure has following form

$$\rho_b^u(k) = K_{\rho_b}^E(k)\xi(k) + K_{\rho_b}^T(k)T_s(k) + K_{\rho_b}^f(k)T_{f0}. \tag{16}$$

where $K_{\rho_b}^E(k)$ and $K_{\rho_b}^T(k)$ are feedback control gain matrices and $K_{\rho_b}^f(k)$ is a feedforward gain vector to compensate the effect of measured disturbance T_{f0}. In this section, we approximate these gains and present simple proportional balancing controller, see Fig. 2(b). This approximation is achieved by exploring properties of gain matrices. This study reveals certain functional properties, control gain structure, and balancing rules, which we present below.

4.1 Balancing Control Gain Structure

Feedback Gains: Let us define a right invertible matrix

$$M_{\rho_b} := \left(M_{\rho_b}^1 - M_{\rho_b}^2\right) \in \mathbb{R}^{n-1\times n}, \tag{17}$$

where $M_{\rho_b}^1 = [0_{n-1}\ I_{n-1}]$ and $M_{\rho_b}^2 = \frac{1}{n}1_{n-1\times n}$. It maps states to *SOC and temperature error vectors*

$$e_{\xi'}(k) = \xi'(k) - \bar{\xi}(k)\cdot 1_{n-1} = M_{\rho_b}\xi(k), \tag{18}$$

$$e_{T_s'}(k) = T_s'(k) - \bar{T}_s(k)\cdot 1_{n-1} = M_{\rho_b}T_s(k), \tag{19}$$

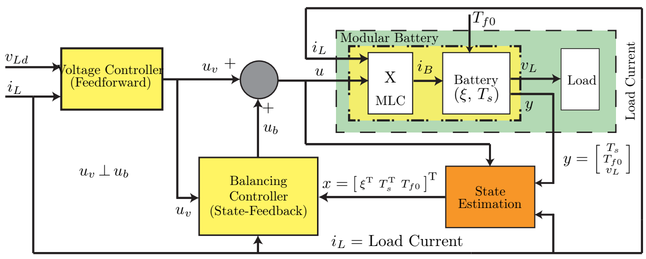

(a) Block diagram of battery control system.

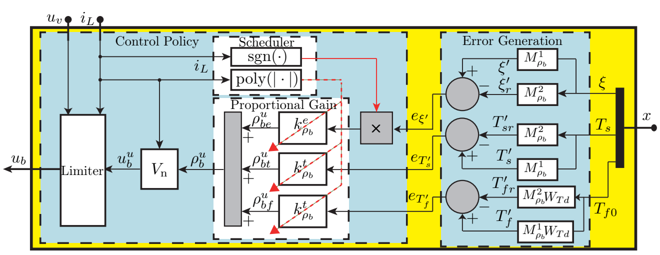

(b) Balancing controller structure: Proportional controller

Fig. 2. Block diagram of closed-loop control system of MLC-based modular battery powering a variable load.

where $\xi'(k) \in \mathbb{R}^{n-1}$ and $T_s'(k) \in \mathbb{R}^{n-1}$ are SOC and temperature of cells 2 to n. Since the objective function in problem (P-I) penalizes state errors, it is reasonable to assume that the control gains given by (13) should also act on state errors $e_{\xi'}(k)$ and $e_{T_s'}(k)$. The empirical study of (13) for small parametric variations suggests following approximate factorization of the feedback gain matrices

$$K_{\rho_b}^E(k) \approx L_{\rho_b}^E(k)M_{\rho_b}, \tag{20}$$

$$K_{\rho_b}^T(k) \approx L_{\rho_b}^T(k)M_{\rho_b}, \tag{21}$$

where the invertible matrices $L_{\rho_b}^E(k) = [\ell_{ij}^e(k)]$ and $L_{\rho_b}^T(k) = [\ell_{ij}^t(k)]$ of order $(n-1)\times(n-1)$ are time-varying control gains for SOC and temperature errors respectively. These time-varying gains have special structure with following properties (explored using empirical study)

- In case of *zero parametric variations* (i.e. $C_{ei} = C_{ej}, R_{ei} = R_{ej}$), the matrices are purely diagonal, each with equal diagonal elements.
- In case of parametric variations, the matrices becomes non-diagonal. However, they are still *diagonally dominant*, for most *practical parametric variations* (20% in capacity and 100% in resistance), with order of magnitude difference between diagonal and non-diagonal entries i.e. $|\ell_{ii}^e| \gg |\ell_{ij}^e|$, $|\ell_{ii}^t| \gg |\ell_{ij}^t|$.
- The diagonal entries are almost equal ($\ell_{ii}^e \approx \ell_{jj}^e$, $\ell_{ii}^t \approx \ell_{jj}^t$) for *small parametric variations.*
- The sign of ℓ_{ii}^e is same as sign of i_L, whereas sign of ℓ_{ii}^t is always negative.
- The magnitudes of $\ell_{jj}^e(k)$ and $\ell_{jj}^t(k)$ have significance dependence on load current $i_L(k)$.

Based on these properties, we have $L_{\rho_b}^E \approx \text{sgn}(i_L)k_{\rho_b}^e I_{n-1}$ and $L_{\rho_b}^T \approx -k_{\rho_b}^t I_{n-1}$ where $k_{\rho_b}^e (\approx |\ell_{ii}^e|) > 0$ and $k_{\rho_b}^t (\approx |\ell_{ii}^t|) > 0$ are scalar gains. This leads us to following approximations of feedback control gains

$$K_{\rho_b}^E(k) \approx \text{sgn}(i_L(k))k_{\rho_b}^e(k)M_{\rho_b}, \tag{22}$$

$$K_{\rho_b}^T(k) \approx -k_{\rho_b}^t(k)M_{\rho_b}. \tag{23}$$

Feedforward Gain: The feedforward gain $K_{\rho_b}^f(k)$, for small resistance variations, has the following factorization

$$K_{\rho_b}^f(k) \approx -k_{\rho_b}^t(k)M_{\rho_b}W_{Td}, \tag{24}$$

with the same scalar gain $k_{\rho_b}^t(k)$ as in (23). Here $W_{Td} = hW_T$ (h is sampling interval and $W_T = [w_{ti}] \in \mathbb{R}^n$) is the T_{f0} influence vector where each w_{ti} describes the influence of T_{f0} on each Cell$_i$. The matrix M_{ρ_b} operates on $W_{Td}T_{f0}$ and computes *ambient temperature error vector*

$$e_{T_f'}(k) = \left(W_{Td}' - \overline{W}_{Td}\cdot 1_{n-1}\right)T_{f0} = M_{\rho_b}W_{Td}T_{f0}, \tag{25}$$

where $T_f' \in \mathbb{R}^{n-1}$ and $W_{Td}' \in \mathbb{R}^{n-1}$ are ambient temperature and T_{f0} influence vector of cells 2 to n, $\overline{W}_{Td} = \frac{1}{n}1_n^{\mathrm{T}}W_{Td}$ is mean influence of T_{f0} on string of cells. The ambient error for each Cell$_i$ is then given by

$$e_{T_{fi}} = \left(w_{ti} - \overline{W}_{Td}\right)T_{f0}. \tag{26}$$

Note that "≈" should be replaced with "=" in (22)–(24) under zero parametric variations.

From (22), (23), and (24), we get the following (approximate) balancing control laws for each Cell$_i$ ($i \in \{2, \cdots, n\}$)

$$u^u_{bei}(k) = \rho^u_{bei}(k) \approx \mathrm{sgn}(i_L(k)) k^e_{\rho_b}(k) e_{\xi_i}(k), \quad (27)$$
$$u^u_{bti}(k) = \rho^u_{bti}(k) \approx -k^t_{\rho_b}(k) e_{T_{si}}(k), \quad (28)$$
$$u^u_{bfi}(k) = \rho^u_{bfi}(k) \approx -k^t_{\rho_b}(k) e_{T_{fi}}, \quad (29)$$

where $e_{\xi_i}(k), e_{T_{si}}(k)$, and $e_{w_{ti}}$ are defined in (10), (11), and (26) respectively. Note that (27)–(29) are balancing control laws for any $n-1$ cells (assumed as cells 2 to n here), whereas the control law of Cell_1 is given by

$$u^u_{b1}(k) = V'_n(k)\rho^u_b(k) = V'_n(k) K_{\rho_b}(k) x(k), \quad (30)$$

which can be verified by studying (14) and (12), where $V'_n(k)$ is defined in (B.2). The control law (30) shows dependence of u^u_{b1} on control of other $n-1$ cells. This is also obvious from the fact that balancing control does not influence the battery terminal voltage i.e. $D_v(k)u_b(k) = v_{Lb}(k) = 0$. This implies that control of any Cell_i can be represented as a linear combination of other controls.

Interpretation of Balancing Rules: Note that the SOC balancing rule (27) during charging and discharging are complement of each other. This makes sense because, to achieve SOC balancing, any Cell_i with positive (negative) SOC error must be discharged more (less) during discharging and must be charged less (more) during charging. The thermal balancing rule (28) is same during both charging and discharging because current through a cell, regardless of its direction, always generate heat (i.e. cannot consume it). The disturbance compensation rule (29) only cancels out the ambient temperature errors for each cell. It makes sense because it is not required to completely cancel out the disturbance itself for balancing.

Note that if any cell has same error sign for both SOC and temperature during discharging then it will have conflicting usage requirements to achieve simultaneous thermal and SOC balancing. In this situation, controller will benefit from short regeneration/charging phase, otherwise it will have to prioritize one of the two objectives. This trade-off can be established based on load current magnitude.

4.2 Proportional Control with Gain Scheduling (PwGS):

The control gains $k^e_{\rho_b}$ and $k^t_{\rho_b}$, for a battery with n *nominal cells*, are given by the following polynomials

$$k^e_{\rho_b}(k) = a_5|i_L(k)|^5 + \cdots + a_1|i_L(k)| + a_0, \quad (31)$$
$$k^t_{\rho_b}(k) = b_5|i_L(k)|^5 + \cdots + b_1|i_L(k)| + b_0, \quad (32)$$

which are identified by fitting curve to control gain data in the following fashion:

- Find $K_{\rho_b}(k)$ for each $i_L(k)$, varying as a ramp function in the interval $[-20c, 20c]$, by solving Riccati equation (13), where c stands for c-rate of current.
- Perform factorization (22)–(24). This gives us data points for gains $k^e_{\rho_b}$ and $k^t_{\rho_b}$ as function of i_L.
- Fitting curve to these data points, we identify coefficients of polynomials (31) and (32).

The gains $k^e_{\rho_b}$ and $k^t_{\rho_b}$, for a battery with 4 nominal cells, are plotted in Fig. 3(a) as a function of $i_L \in [-20c, 20c]$ and the coefficients are given in Table 2. The gain curves show clear trade-off between thermal and SOC balancing objectives. Each of these objectives is prioritized in different load current range. For example, SOC balancing is prioritized for $|i_L| \leq 8\,c$ and thermal balancing is prioritized in $|i_L| > 8\,c$. This behavior makes sense because thermal balancing is not much needed during low current intervals due to reduced thermal intensity. These *two dominant control modes* show that the simultaneous thermal and SOC balancing is not possible for continuously high load.

Table 2. Coefficients of Gain Polynomials

Params.	**Value**	**Params.**	**Value**
a_5	-2.460×10^{-6}	b_5	-4.063×10^{-8}
a_4	3.560×10^{-4}	b_4	7.753×10^{-6}
a_3	-0.015	b_3	-5.224×10^{-4}
a_2	0.012	b_2	0.0132
a_1	8.740	b_1	-0.038
a_0	-0.759	b_0	0.0430

4.3 Proportional with Simple Balancing Rules (PwSBR):

Considering two dominant control behaviors in two different current ranges, we can motivate even simpler balancing rules/policy as given below and shown in Figure 3(b).

$$k^e_{\rho_b}(k) = \begin{cases} \mathrm{sgn}(i_L(k)) \cdot 60, & \text{if } |i_L(k)| \leq 8\,c \\ \mathrm{sgn}(i_L(k)) \cdot 20, & \text{otherwise.} \end{cases} \quad (33)$$

$$k^t_{\rho_b}(k) = \begin{cases} 0.25, & \text{if } |i_L(k)| \leq 8\,c \\ 3.6, & \text{otherwise.} \end{cases} \quad (34)$$

The above rules capture the main essence of balancing controller i.e. if $|i_L| \leq 8\,c$, prioritize SOC balancing, else thermal balancing.

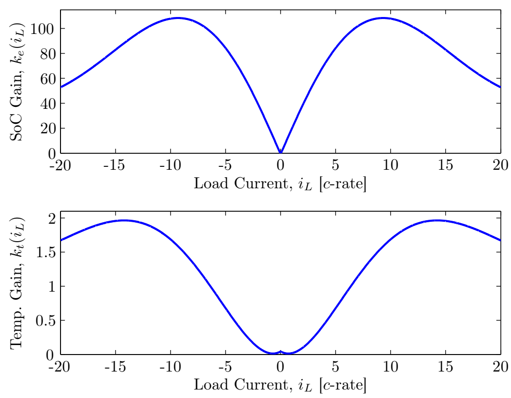

(a) Continuous gain scheduling (PwGS)

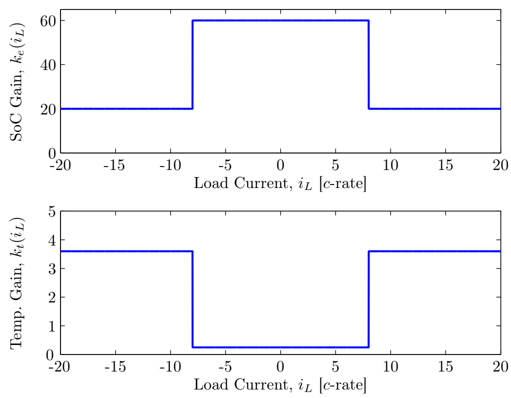

(b) Simple balancing gains/rules (PwSBR).

Fig. 3. Proportional gains as function of load current i_L.

4.4 Control Limiter

The balancing control limiter, originally formulated as problem (P-II), is approximated using Algorithm 1 for easier implementation. It achieves $u_b \in \mathcal{U}_b$ by successively applying the following two Euclidean projections of unconstrained control until convergence of control error ε_{u_b}.

- Projection on box $\mathcal{U}_{b1}$ to satisfy $u_b \in [u_{b,\min}, u_{b,\max}]$ (lines 4—7).
- Projection on hyperplane $\mathcal{N}(D_v)$ to satisfy $v_L = v_{Ld}$ (lines 8—10).

Note that we use analytical solutions for projections on rectangle and hyperplane (see Boyd and Vandenberghe (2006)). The solution is optimal (equivalent to solving (P-II)) for $n = 2$, but may get suboptimal for $n > 2$.

Algorithm 1 Control Limiter

1: **Given**: $u_b^u(k), u_{b,\min}(k), u_{b,\max}(k), D_v(k)$, tol.
2: **Set** $i = 1,\quad u_b^i = u_{b,u},\quad \varepsilon_{u_b}^0 = 1_n$ ▷ Initialize
3: **while** $\left(\varepsilon_{u_b}^{i-1} \geq \text{ tol}\right)$ **do**
▷ Find limit violations
4: $\quad I_{u_b}^{\text{vl}} = \texttt{find}(u_b^i < u_{b,\min})$
5: $\quad I_{u_b}^{\text{vu}} = \texttt{find}(u_b^i > u_{b,\max})$
▷ Project on box
6: $\quad u_b^i(I_{u_b}^{\text{vl}}) = u_{b,\min}(I_{u_b}^{\text{vl}})$
7: $\quad u_b^i(I_{u_b}^{\text{vu}}) = u_{b,\max}(I_{u_b}^{\text{vu}})$
▷ Project on hyperplane
8: $\quad \varepsilon_{v_{Lb}}^i = 0 - D_v u_b^i$ ▷ voltage error
9: $\quad \varepsilon_{u_b}^i = \varepsilon_{v_{Lb}}^i D_v^\dagger$ ▷ balancing control error
10: $\quad u_b^{i+1} = u_b^i + \varepsilon_{u_b}^i$ ▷ Correction/Update equation
11: $\quad i \leftarrow i + 1$
12: **end while**
13: **return** u_b

5. SIMULATION RESULTS AND DISCUSSION

5.1 Simulation Setup

We evaluate, through simulations, the balancing performance of two proposed proportional controllers (PwGS and PwSBR) and compare it with one-step MPC for *US06* drive cycle (representative of intensive driving). We must reemphasize here that the MPC, with the same setting as in Altaf et al. (2015a), uses true cell parameters, but the proportional controllers are implemented assuming only nominal parameter values. All three controllers use sampling interval $h = 1\,\text{sec}$. Note that we do not require any special solvers for proportional controllers. However, for MPC, we need a QP solver like `CVX` (Boyd and Vandenberghe (2006), Grant and Boyd (2011)) to solve Euclidean projection problem (P-II).

The modular battery considered for this study consists of 4 modules, each containing one cell (3.3V, 2.3Ah, A123 ANR26650M1A). The nominal values of cell's electro-thermal parameters have been taken from Lin et al. (2013b) and the coolant inlet temperature T_{f0} is assumed constant at 25°C. The true cells are assumed to have capacity, SOC, and resistance variations as shown in Figure 4. The battery load current data for US06 were obtained at 1 Hz by simulation of Toyota Prius PHEV in full EV mode in *Advisor* (Wipke et al. (1999)). We assume $v_{Ld} = 9.25\,V$ (battery load voltage demand at dc-link).

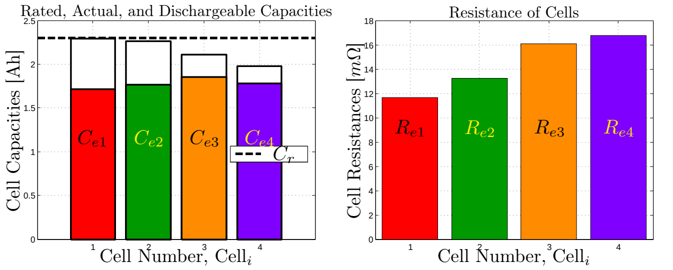

(a) Variation in cell capacities. (b) Variation in cell resistances.

Fig. 4. Figure shows capacity and resistance distribution of cells. Figure 4(a) shows variation in actual and dischargeable capacities, $C_{ed,i}(k) = \xi_i(k)C_{ei}$, along with rated capacity C_r of cells.

5.2 Comparison of Balancing Performance

The simulation results for two driving trips of US06 are shown in Figure 5. The plots are arranged in a 3×3 matrix of subfigures where columns correspond to MPC, PwGS, and PwSBR respectively and each row corresponds to one of three battery performance variables: $\xi(k), T_s(k)$, and $\{\|e_\xi(k)\|_\infty, \|e_{T_s}(k)\|_\infty\}$. These plots clearly show that all three controllers significantly reduce SOC deviation among cells relative to the initial condition. Initially, the SOC deviation monotonically decreases almost all the time as shown in Figures 5(g), 5(h), and 5(i). After decay of initial SOC imbalance, all controllers are able to keep tight equalization of SOCs ($\leq 1\%$), while keeping temperature deviations within almost 1°C during both charging and discharging. The performance statistics show that PwGS gives almost similar performance as MPC. The PwSBR gives lower peak in $e_{T_s}(k)$, but at the expense of slower SOC balancing and slightly higher mean and standard deviation of both thermal and SOC imbalance.

5.3 Comparison of Computational Efficiency

The computational times (obtained on a PC with i7 processor and 16 GB RAM) for two stages (gain computation and projections) of each balancing controller are shown in Table 3. We save a lot of computational time during the second stage of proportional controllers. There is no significant difference for first stage due to small size of problem in this simulation. However, for large n, the computation time of first stage for MPC will grow significantly due to matrix inversion in Riccati equation (13) as shown in Figure 6.

Table 3. Computational Efficiency Comparison

Online Timing	**MPC**	**PwGS**	**PwSBR**
Control Computation	50 μs	40 μs	23 μs
Control Projection	150 ms	1.2 ms	1.2 ms

6. SUMMARY AND CONCLUSIONS

In our earlier study (Altaf et al. (2015a)), we proposed LQ MPC based balancing controller with two stages to solve

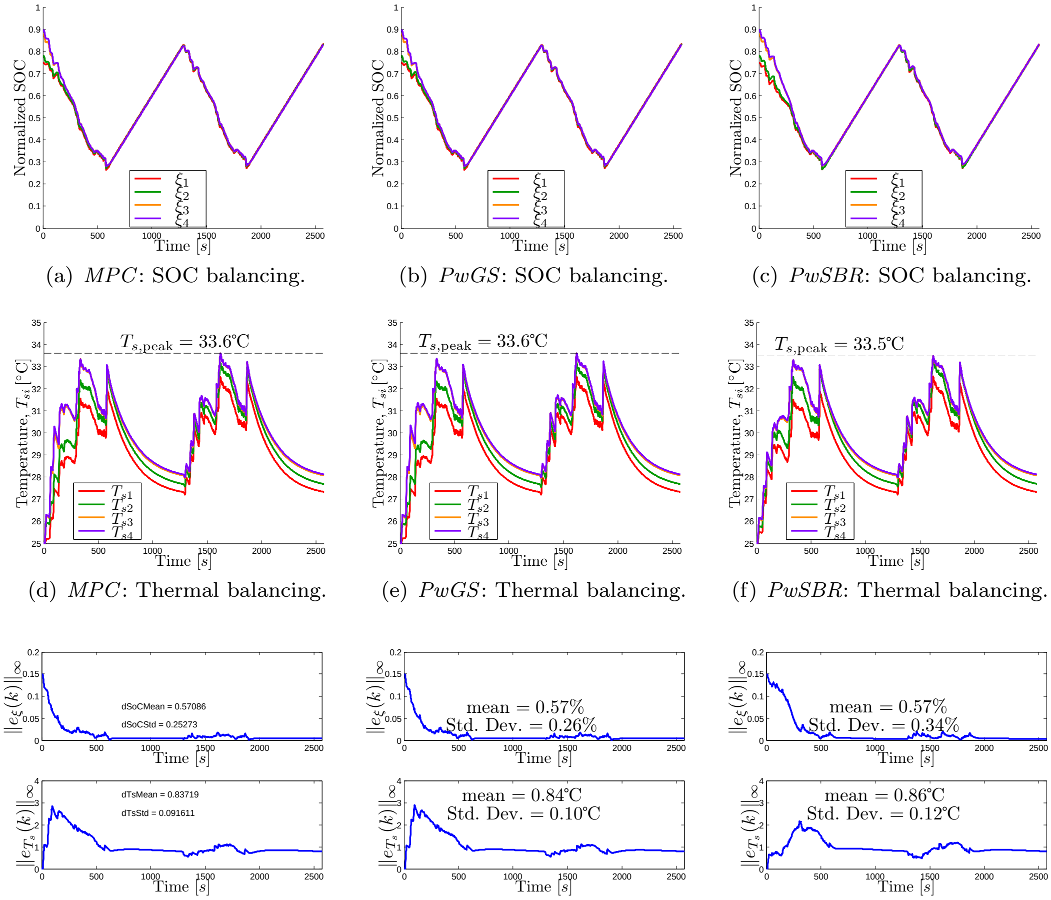

(a) *MPC*: SOC balancing. (b) *PwGS*: SOC balancing. (c) *PwSBR*: SOC balancing.

(d) *MPC*: Thermal balancing. (e) *PwGS*: Thermal balancing. (f) *PwSBR*: Thermal balancing.

(g) *MPC*: Balancing errors. (h) *PwGS*: Balancing errors. (i) *PwSBR*: Balancing errors.

Fig. 5. Simulation results for balancing performance of modular battery under *US06 drive cycle* are shown: first column: 1-step *Constrained MPC Scheme*; second column: *PwGS with Limiter*; and third column: *PwSBR with Limiter*.

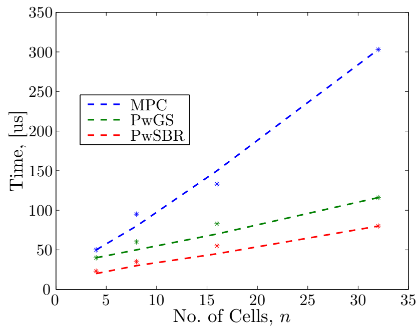

Fig. 6. Computational time versus no. of cells, n.

thermal and SOC balancing problem of a modular battery. The first stage computes time-varying LQ control gains and second stage performs Euclidean control projections to satisfy control constraint.

This paper is an extension of Altaf et al. (2015a). The main purpose was to propose a simple proportional balancing controller by studying the structural properties of LQ control gains. In addition, we aimed to solve projection problem using simpler algorithm. This study discovered that, under the assumption of small cell parametric variations, each time-varying control gain matrix can be factorized into a constant matrix and a time-varying scalar gain. We identified two scalar gains (one for SOC and the other for thermal balancing) as 5^{th} order polynomials in load current. We also proposed simple iterations to compute projections. These approximations result in a simple and computationally efficient proportional balancing controller, which can be easily implemented on low-power embedded hardware as it does not require solving any optimization problem. The study has also revealed two dominant modes of balancing controller i.e. SOC balancing in low current range and thermal balancing in high current range. Using this insight, we also proposed another rule-based proportional balancing controller, capturing these two modes.

The performance of balancing controllers have been thoroughly evaluated and compared with one-step MPC for a four cell battery with parametric variations. Although, both proportional controllers have been implemented assuming battery with zero parametric variations, we still get balancing performance comparable to MPC, which assumes full access to true battery parameters. The performance is promising in this simulation case study, but need experimental validation on large battery packs.

7. ACKNOWLEDGMENTS

The authors would like to thank Lars Johannesson for all the positive discussions while developing this work.

Appendix A. STATE-SPACE SYSTEM MATRICES

The matrices for model (4a)–(4b) are given by

$$A = \begin{bmatrix} A_E & 0 \\ 0 & A_\vartheta \end{bmatrix},\ B(i_L(t)) = \begin{bmatrix} B_E i_L \\ B_\vartheta i_L^2 \end{bmatrix},$$

$$A_E = 0_{n\times n},\ B_E = -\frac{1}{3600}\mathrm{diag}\,(b_{e1},\cdots,b_{en}) \in \mathbb{R}^{n\times n},$$

$$A_\vartheta = \begin{bmatrix} A_T & W_T \\ 0_n^{\mathrm{T}} & 0 \end{bmatrix},\quad B_\vartheta = \begin{bmatrix} B_T \\ 0_n^{\mathrm{T}} \end{bmatrix},$$

$$A_T = [a_{tij}] \in \mathbb{R}^{n\times n},\quad B_T = \mathrm{diag}\,(b_{t1},\cdots,b_{tn}) \in \mathbb{R}^{n\times n},$$

$$W_T = [w_{t1}\ \cdots\ w_{tn}]^{\mathrm{T}} \in \mathbb{R}^n,$$

$$C = \begin{bmatrix} 0 & I_{n+1} \\ 0_n^{\mathrm{T}} & 0_{n+1}^{\mathrm{T}} \end{bmatrix},\ D(i_L(t)) = \begin{bmatrix} 0 \\ D_v(t) \end{bmatrix},$$

$$D_v(t) = [d_{v1}(t)\ \cdots\ d_{vn}(t)] \in \mathbb{R}^{1\times n},$$

where A_T is a constant lower triangular thermal subsystem matrix and the coefficients $b_{ei} = \frac{1}{C_{ei}}$ and $b_{ti} = \frac{R_{ei}}{C_{si}}$. Note that $D_v(t)$ is a feedthrough gain from $u(t)$ to $v_L(t)$.

Appendix B. SET DEFINITIONS

The nullspace of $D_v(k)$ is a hyperplane in $\mathbb{R}^n$ given by

$$\mathcal{N}(D_v) = \{u(k)|D_v(k)u(k) = 0\} = \mathcal{R}(V_{\mathrm{n}}) \subseteq \mathbb{R}^n, \quad \text{(B.1)}$$

where $\mathcal{R}(V_{\mathrm{n}})$ is the range-space of null-space basis matrix

$$V_{\mathrm{n}}(k) = \begin{bmatrix} V'_{\mathrm{n}}(k) \\ I_{n-1} \end{bmatrix} \in \mathbb{R}^{n\times n-1},\quad V'_{\mathrm{n}}(k) = \frac{-1}{d_{vi}(k)} D'_v(k) \quad \text{(B.2)}$$

where $D'_v \in \mathbb{R}^{1\times n-1}$ is obtained by deleting 1^{st} element of D_v. Using (7), (8), and (B.1), we define

$$\mathcal{U}_b(k) = \mathcal{U}_{b1}(k) \cap \mathcal{N}(D_v(k)), \quad \text{(B.3)}$$

where $\mathcal{U}_{b1}(k) = \{u_b(k)\,|\,H_{u_b}u_b(k) \le b_{u_b}(k)\}$ is a box constraint with matrix $H_{u_b} = H_u$ and time-varying vector

$$b_{u_b}(k) = \left[-u_{b,\min}{}^{\mathrm{T}}\ u_{b,\max}{}^{\mathrm{T}}\right]^{\mathrm{T}} = h_u - H_u u_v(k). \quad \text{(B.4)}$$

REFERENCES

Altaf, F., Egardt, B., and Johannesson, L. (2015a). Electro-thermal Control of Modular Battery using Model Predictive Control with Control Projections. In *IFAC Workshop on Engine and Powertrain Control, Simulation and Modeling, 2015*, volume 48, 368 – 375.

Altaf, F., Johannesson, L., and Egardt, B. (2014). Simultaneous Thermal and State-of-Charge Balancing of Batteries: A Review. In *Vehicle Power and Propulsion Conference (VPPC), 2014 IEEE*, 1–7. doi:10.1109/VPPC.2014.7007132.

Altaf, F., Johannesson, L., and Egardt, B. (2012). Evaluating the Potential for Cell Balancing using a Cascaded Multi-Level Converter using Convex Optimization. In *IFAC Workshop on Engine and Powertrain Control, Simulation and Modeling, 2012*.

Altaf, F. (2014). *Thermal and State-of-Charge Balancing of Batteries using Multilevel Converters*. Licentiate Thesis, Chalmers University of Technology. URL `http://publications.lib.chalmers.se/records/fulltext/194660/194660.pdf`.

Altaf, F., Egardt, B., and Johannesson, L. (2015b). Load Management of Modular Battery using Model Predictive Control: Thermal and State-of-Charge Balancing (Submitted to IEEE Transactions on Control Systems Technology). Preprint available at `http://publications.lib.chalmers.se/records/fulltext/228087/local_228087.pdf`.

Altaf, F., Johannesson, L., and Egardt, B. (2013). On Thermal and State-of-Charge Balancing using Cascaded Multi-level Converters. *Journal of Power Electronics*, 13(4), 569–583.

Bandhauer, T.M., Garimella, S., and Fuller, T.F. (2011). A critical review of thermal issues in lithium-ion batteries. *Journal of the Electrochemical Society*, 158(3), R1–R25.

Barreras, J., Pinto, C., and et.al. (2014). Multi-objective control of balancing systems for li-ion battery packs: A paradigm shift ? In *Vehicle Power and Propulsion Conference (VPPC), 2014 IEEE*.

Boyd, S. and Vandenberghe, L. (2006). *Convex Optimization*. Cambridge University Press.

Cao, J., Schofield, N., and Emadi, A. (2008). Battery balancing methods: A comprehensive review. In *Vehicle Power and Propulsion Conference, 2008. VPPC '08. IEEE*, 1 –6.

Dubarry, M., Vuillaume, N., and Liaw, B.Y. (2010). Origins and accommodation of cell variations in li-ion battery pack modeling. *International Journal of Energy Research*, 34(2), 216–231.

Gallardo-Lozano, J., Romero-Cadaval, and et.el. (2014). Battery equalization active methods. *Journal of Power Sources*, 246, 934–949.

Grant, M. and Boyd, S. (2011). CVX: Matlab software for disciplined convex programming, version 1.21.

Groot, J. (2014). *State-of-Health Estimation of Li-ion Batteries: Ageing Models*. PhD Thesis. New Series, no: 3815. Chalmers University of Technology,.

Hu, X., Li, S., and Peng, H. (2012). A comparative study of equivalent circuit models for li-ion batteries. *Journal of Power Sources*, 198(0), 359 – 367.

Lin, X., Fu, H., Perez, H.E., and et.el. (2013a). Parameterization and observability analysis of scalable battery clusters for onboard thermal management. *Oil & Gas Science and Technology–Revue d'IFP Energies nouvelles*, 68(1), 165–178.

Lin, X., Perez, H., Siegel, J., Stefanopoulou, A., and et.el. (2013b). Online parameterization of lumped thermal dynamics in cylindrical lithium ion batteries for core temperature estimation and health monitoring. *Control Systems Technology, IEEE Transactions on*, 21(5), 1745–1755.

Lu, L., Han, X., Li, J., Hua, J., and Ouyang, M. (2013). A review on the key issues for lithium-ion battery management in electric vehicles. *Journal of Power Sources*, 226, 272–288.

Mahamud, R. and Park, C. (2011). Reciprocating air flow for li-ion battery thermal management to improve temperature uniformity. *Journal of Power Sources*, 196(13), 5685 – 5696.

Malinowski, M., Gopakumar, K., Rodriguez, J., and Pérez, M. (2010). A survey on cascaded multilevel inverters. *Industrial Electronics, IEEE Transactions on*, 57(7), 2197 –2206.

Vetter, J., Novak, P., Wagner, M., and et.el. (2005). Ageing mechanisms in lithium-ion batteries. *Journal of power sources*, 147(1), 269–281.

Wang, J., Liu, P., Hicks-Garner, and et.el. (2011). Cycle-life model for graphite-$LiFePO_4$ cells. *Journal of Power Sources*, 196(8), 3942–3948.

Wipke, K., Cuddy, M., and Burch, S. (1999). Advisor 2.1: a user-friendly advanced powertrain simulation using a combined backward/forward approach. *Vehicular Technology, IEEE Transactions on*, 48(6), 1751–1761.